23rd ABCM International Congress of Mechanical Engineering
December 6-11, 2015, Rio de Janeiro, RJ, Brazil

EVALUATION OF THE SPECTRAL DIFFERENCE METHOD FOR INVISCID COMPRESSIBLE FLOWS

Fábio Mallaco Moreira
Carlos Breviglieri
Instituto Tecnológico de Aeronáutica, São José dos Campos, SP, Brazil
fabiom91@gmail.com, carbrevi@gmail.com

João Luiz F. Azevedo
Instituto de Aeronáutica e Espaço, São José dos Campos, SP, Brazil
joaoluiz.azevedo@gmail.com

Abstract. *In this paper the authors present an evaluation of the spectral difference method (SD) for the resolution of two dimensional inviscid compressible flows. The high-orde method is coupled with a high-order discontinuity marker and a hierarchical limiting procedure in order to preserve numerical stability near shock waves in transonic flows. The evaluation is composed of an order of accuracy assesment performed in the Ringleb flow problem, referece transonic aeronautical flows over airfoils and a supersonic flow over a wedge. Results of the airfoil simulations are comapred with other high orde methods and wedge flow results provide data about the marker and limiter capabilities.*

Keywords: *Spectral Difference; High-order scheme; Unstructured meshes; Transonic; Aerodynamic applications*

1. INTRODUCTION

There is an active research community working on high-order methods for unstructured meshes. The international workshops on high-order CFD methods (Wang *et al.*, 2013) have gathered several research groups to discuss and propose solutions for the difficulties encountered in high-order simulations for practical aerospace applications. Among such difficulties, one can cite the solution discontinuity treatment, which may reduce the order of accuracy of the solution, robust and efficient time integration algorithms and mesh flexibility towards an efficient high-order solution. These topics are deemed worth of future research to allow the full exploitation of high-order methods by the general CFD community.

The interest in the spectral difference (SD) method was prompted by the limitations encountered by the research group with other high order methods, namely the Spectral Finite Volume (SFV) and the Weighted Essentially Non-Oscillatory (WENO) schemes. The SFV method is restricted to triangular meshes, in 2-D, which limit its capability to capture boundary layer effects. The WENO schemes, on the other hand, present a very high computational cost and are difficult to efficiently implement in parallel. These limitations are expected to be overcome with the SD method since it is based on quadrilateral grids and have simple and straightforward implementation.

2. SPECTRAL DIFFERENCE METHOD FORMULATION

The Euler equations describe the most general flow configuration for a non- viscous, non-heat conducting fluid. They can be obtained by neglecting all viscous stresses and heat conduction terms present in the Navier-Stokes equations. When considering the above hypothesis, the resulting system of partial differential equations reduces to a first order system. In the present work, the 2-D Euler equations are solved in their differential form as

$$\frac{\partial Q}{\partial t} + \frac{\partial E}{\partial x} + \frac{\partial F}{\partial y} = 0\,. \tag{1}$$

The vector of conserved variables, Q, and the convective flux vectors, E and F, are given by

$$Q = \begin{Bmatrix} \rho \\ \rho u \\ \rho v \\ \varepsilon \end{Bmatrix}, \quad E = \begin{Bmatrix} \rho u \\ \rho u^2 + p \\ \rho u v \\ (\varepsilon + p)u \end{Bmatrix}, \quad F = \begin{Bmatrix} \rho v \\ \rho u v \\ \rho v^2 + p \\ (\varepsilon + p)v \end{Bmatrix}. \tag{2}$$

The system is closed by the equation of state for a perfect gas

$$p = (\gamma - 1)\left[\varepsilon - \frac{1}{2}\rho(u^2 + v^2)\right], \tag{3}$$

where ε is the total energy per unit volume and the ratio of specific heats, γ, is set as 1.4 for all computations in the present work.

The Spectral Difference method (SD) employs a finite difference-like scheme and, to achieve an efficient implementation, all elements in the physical domain, (x, y), are transformed into a unit square element in the computational domain. Such transformation can be written as

$$\begin{pmatrix} x \\ y \end{pmatrix} = \sum_{s=1}^{K} M_s(\xi, \eta) \begin{pmatrix} x_s \\ y_s \end{pmatrix} , \tag{4}$$

where K is the number of points used to define the physical element, (x_s, y_s) are the Cartesian coordinates of these points, and $M_s(\xi, \eta)$ are the shape functions of the geometric transformation. In the case of a 1st-order linear boundary mesh, the transformation is bilinear and the analytic expression can be easily found. However, in the case of higher order meshes, required to represent accurately curved geometries, the number of points used to define a single cell increases. Considering a bi-polynomial representation, the transformation parameters can be calculated by numerically solving a linear system of size K. The metrics and the Jacobian matrix of the transformation can be computed in a pre-processing step and kept in memory given the stationary aspect of the mesh for the problems here considered. The implementation follows the formulation presented in Wang *et al.* (2007) and May and Jameson (2006). The governing equations in the physical domain are, then, transferred into the computation domain, and they are rewritten as

$$\frac{\partial \tilde{Q}}{\partial t} + \frac{\partial \tilde{E}}{\partial \xi} + \frac{\partial \tilde{F}}{\partial \eta} = 0 \, , \tag{5}$$

where $\tilde{Q} = |J| \cdot Q$ and the flux vectors in the computational domain can be simplified from the general form as

$$\begin{pmatrix} \tilde{E} \\ \tilde{F} \end{pmatrix} = |J| \cdot \begin{pmatrix} \xi_x & \xi_y \\ \eta_x & \eta_y \end{pmatrix} \begin{pmatrix} E \\ F \end{pmatrix} = \begin{pmatrix} x_\xi & x_\eta \\ y_\xi & y_\eta \end{pmatrix}^{-1} \begin{pmatrix} E(\tilde{Q}) \\ F(\tilde{Q}) \end{pmatrix} . \tag{6}$$

where J is the Jacobian matrix of the coordinate transformation given by

$$J = \begin{pmatrix} x_\xi & x_\eta \\ y_\xi & y_\eta \end{pmatrix} . \tag{7}$$

In the standard element, two sets of points are defined, namely the solution points (SP) and the flux points (FP), as shown in Fig. 1. The stability of the method in a large array of problems is independent from the distribution of the SPs (van den Abeele *et al.*, 2008), meaning another criteria may be used in order to determine the location of these points. If, for instance, memory usage is a concern, SPs could be made to coincide with FPs, hence minimizing memory allocation. In the present implementation, the favored aspects were simplicity of implementation and computational efficiency, more detail on the implementation used can be seen in Moreira *et al.* (2015). The present work considers an explicit Runge-Kutta scheme for time marching. The 3rd-order, 4-stage optimal strong stability preserving Runge-Kutta scheme, described in Spitieri and Ruuth (2003), is implemented.

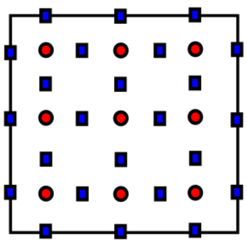

Figure 1. Possible flux point (blue squares) and solution point (red circles) distribution for the 3rd-order SD method.

3. LIMITED RECONSTRUCTION

In the context of the Euler formulation, it is necessary to limit some reconstructed properties at flux integration points in order to maintain stability and convergence of the simulation, if the flow solution contains discontinuities. The limiting methodology can be broken down in two steps. The first one consists in computing the values of properties at the flux points in each cell and in marking problematic reconstructions. The second step consists in generating a new reconstruction that guarantees local smoothness of the solution.

The main concern in selecting a marker formulation for this work is that it performs consistently for all orders of reconstruction polynomials and would not enforce limiting of high-order smooth extrema. The AP-TVD marker consists of a two-step process. The first step consists of comparing the values of the primitive variables in each Solution Point (SP), of the cell under consideration, to the maximum and minimum cell-averages of a local stencil. This stencil is composed of the inspected cell and its immediate face neighbors. If a cell SP is not bounded by the local stencil minimum and maximum values, the cell is marked as troubled and it is further considered in the following step.

This initial selection inevitably marks all local maximum and minimum properties, regardless of whether they are undesired oscillations or smooth extrema. In an attempt to unmark the false positives, that is, local maximum and minimum properties which are smooth extrema, derivative data from the local stencil is analyzed. If the SP property extrema are smooth, their first derivatives must be monotonic. In such cases, the second derivatives must be bounded by the slopes of their first-derivatives. Such condition is evaluated with a minmod TVD marker and, when the second derivative is bounded, $\tilde{u}_i^{(2)} = \overline{u}_i^{(2)}$, the cell is unmarked. Here,

$$\tilde{u}_i^{(2)} = minmod\left(\beta\frac{\overline{u}_i^{(1)} - \overline{u}_{i-1}^{(1)}}{x_i - x_{i-1}}, \overline{u}_i^{(2)}, \beta\frac{\overline{u}_{i+1}^{(1)} - \overline{u}_i^{(1)}}{x_{i+1} - x_i},\right) , \tag{8}$$

where the β parameter is set to $\beta = 1.5$, following the suggestions presented in Yang and Wang (2009).

The objective of this limiter formulation is to take advantage of the universal reconstruction used in the SD method. It benefits from the readily available derivative data provided by the usual SD reconstruction. When a cell is indeed marked as a troubled one, the SD method reconstruction polynomial can no longer be used in the discretization process. Another polynomial must be provided for this cell, which respects the monotonicity criteria and stabilizes the discretization in the presence of strong discontinuities. Ideally, this other polynomial should maintain the high-order aspect of the SD method.

The limiting process is recursive and it works by progressively lowering the reconstruction polynomial order until the smoothness criteria, or 1st-order, is achieved. The limited polynomial is constructed based on the troubled cell averaged derivative data. This information is used to generate a numerical series expanded from the centroid of the cell. To illustrate this concept, and considering a one-dimensional reconstruction, the limited polynomial can be written as

$$\begin{aligned} u_i(x) = \overline{u}_i + \overline{u}_i^{(1)}(x - x_i) + \frac{1}{2}\overline{u}_i^{(2)}[(x - x_i)^2 - \frac{1}{12}h_i^2] \\ + \frac{1}{6}\overline{u}_i^{(3)}[(x - x_i)^3 - \frac{1}{4}h_i^2(x - x_i)] + \frac{1}{24}\overline{u}_i^{(4)}[(x - x_i)^4 - \frac{1}{2}h_i^2(x - x_i)^2 + \frac{7}{240}h_i^4] + ... \end{aligned} \tag{9}$$

where x_i is the coordinate of the cell centroid, h_i is a characteristic length of the 1-D cell and $\overline{u}_i$ is the discrete representation of the u_i variable. The $\overline{u}_i^{(p)}$ symbol denotes the p-th derivative of u_i.

The next step is similar to the one described in the AP-TVD marker discussion, and it verifies whether the current p-th order polynomial is bounded by its $p-1$ derivatives. In other words, if the $p-1$ derivative is monotonic, the limited polynomial is not oscillatory. A minmod function is used to perform the limited derivative calculation, represented by $\overline{U}_i$ for a 1-D formulation. The limited derivative can be written as

$$\overline{U}_i^{(p)} = minmod\left(\beta\frac{\overline{u}_i^{(p-1)} - \overline{u}_{i-1}^{(p-1)}}{x_i - x_{i-1}}, \overline{u}_i^{(p)}, \beta\frac{\overline{u}_{i+1}^{(p-1)} - \overline{u}_i^{(p-1)}}{x_{i+1} - x_i},\right) . \tag{10}$$

The process finishes when $\overline{U}_i^p = \overline{u}_i^p$ and, hence, no further limiting is necessary. All derivatives with order lower than p retain their unlimited values. Once the limited reconstruction procedure is finished, a new solution is generated for the SPs. Again, for the sake of illustration, a 1-D limited reconstruction polynomial for the U_i variable is expressed as

$$\begin{aligned} U_i(x) = \overline{U}_i + \overline{U}_i^{(1)}(x - x_i) + \frac{1}{2}\overline{U}_i^{(2)}[(x - x_i)^2 - \frac{1}{12}h_i^2] \\ + \frac{1}{6}\overline{U}_i^{(3)}[(x - x_i)^3 - \frac{1}{4}h_i^2(x - x_i)] + \frac{1}{24}\overline{U}_i^{(4)}[(x - x_i)^4 - \frac{1}{2}h_i^2(x - x_i)^2 + \frac{7}{240}h_i^4] + ... \end{aligned} \tag{11}$$

4. NUMERICAL RESULTS

4.1 Ringleb Flow

The Ringleb flow simulation consists of an isentropic internal flow. It has an analytic solution for the Euler equations which can be derived with the hodograph transformation (Shapiro, 1953). The parameters for the case considered here are based on the test case from the International Workshop on High-Order Methods in CFD (Wang *et al.*, 2013). The flow depends on the inverse of the stream function, k, and the velocity magnitude, v_t. In the present simulations, these parameters are chosen as $k = 0.7$ and $k = 1.5$, in order to define the bounding streamlines, and $v_t = 0.5$ to define the inlet and outlet boundaries. An interesting property of the Ringleb flow test case is that transition of flow regime from supersonic to subsonic is shockless. Simulations of 2nd- through 6th-order SD methods are used to compute the solution for this problem and benchmark the accuracy of the method and implementation. Figure 2 presents Mach number contours from 0.6 to 2.0 at equally spaced levels for the analytic, 2nd-, 3rd- and 4th-order solutions obtained on the same mesh. It should be noticed that this is an extremely coarse grid with only 12 cells and 48, 108, 192 degrees of freedom in the 2nd-, 3rd- and 4th-order solutions, respectively. The 2nd-order case presents severe disturbances and asymmetry, presenting a maximum entropy error of 1.36×10^{-1} and an average error of 2.04×10^{-2}. The 3rd- and 4th-order schemes show significant improvements. The 4th-order scheme presents a maximum entropy error of 1.39×10^{-2} and an average error of order 10^{-4}.

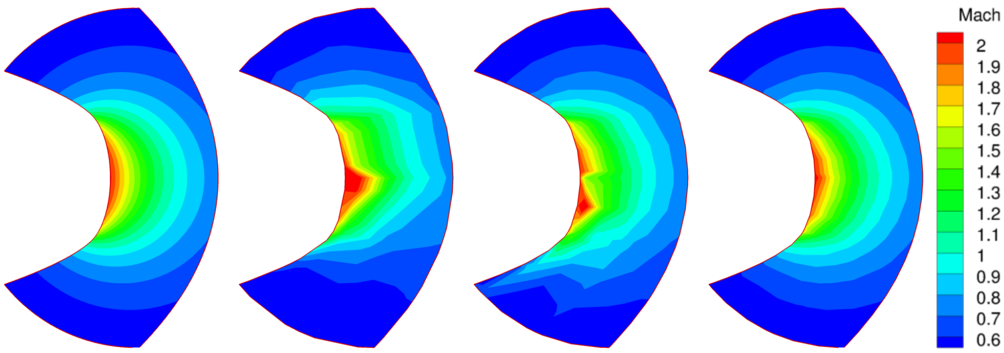

(a) Analytic (b) 2nd-order (c) 3th-order (d) 4th-order

Figure 2. Mach number contours for the Ringleb flow problem.

The results for the SD scheme order analysis can be seen in Fig. 3. The scheme measured orders of accuracy are nearly ideal for 2nd- and 3rd-order reconstructions. However, the expected accuracy is not fully achieved for the 4th-, 5th- and 6th-order methods. Nevertheless, a significant improvement in the flow resolution is observed from one result to another. Further tests indicated that there is an increasingly smaller mesh size interval for which full high-order accuracy can be achieved for the higher-order cases.

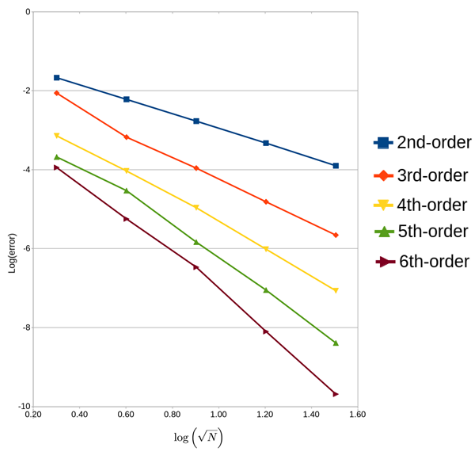

Figure 3. Ringleb flow problem L_1 error visualization.

4.2 NACA 0012 Airfoil

A transonic NACA 0012 airfoil flow simulation is performed with the SD method. The free stream Mach number value of $M_\infty = 0.8$ and $\alpha = 0$ deg. are used in order to match the experiments in McDevitt and Okuno (1985). The mesh is composed of 4619 quadrilateral cells and 108 edges at the airfoil geometry, meshed in a *C*-type grid topology. The geometry of the airfoil is modified to have a collapsed trailing edge. The distance from the airfoil to the farfield is 10 times the chord length.

The 3rd-order SD method with the hierarchical limiter is considered for this study. Figure 4 presents density contours along with the limited cells at the last iteration of the SD simulation. Regardless of the number of limited cells, a reasonably symmetric solution is encountered, as expected in this flow condition. Such result indicates that the troubled cell marker might be overly sensitive. One can note that cells at apparently smooth regions are marked as problematic and, consequently, have their local high-order solution replaced. This sensitivity presents a barrier for numerical convergence as the limited reconstruction tends to increase the local residue at such cells. In fact, the convergence history in Fig. 5(a) shows a stall of the density residual. However, the lift coefficient history, in the same figure, indicates that the solution is close to what one would expect for this flow condition. The authors believe that a high-order boundary representation would improve the convergence rate and also the force computation.

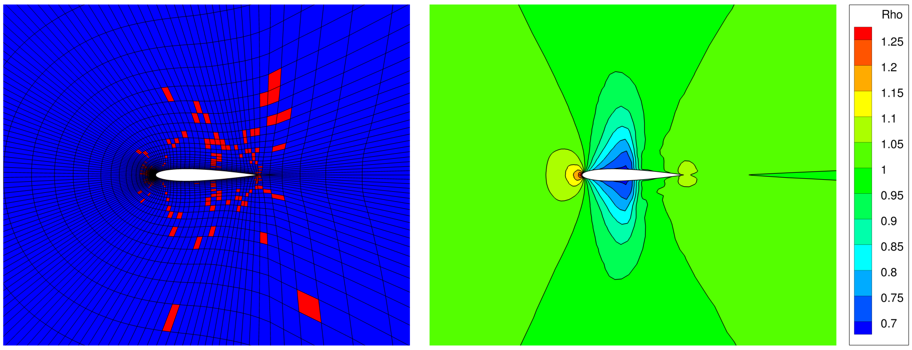

(a) Limited cells for density reconstruction (red). (b) Density contours.

Figure 4. Results for the SD method NACA 0012 airfoil simulations at $M_\infty = 0.8$ and $\alpha = 0$ deg.

A comparison with other high-order methods, namely the weighted essentially non-oscillatory (WENO) (Wolf and Azevedo, 2007), spectral finite volume (SFV) with a minmod limiter and a hybrid SFV-WENO (Breviglieri *et al.*, 2014) methods, is performed. An unstructured grid, composed of 4911 triangles, of which 100 edges define the airfoil geometry, was used for the SFV method simulations. The grid is asymmetric and the distance from the airfoil to the farfield is of 100 chords. For the WENO scheme case, a refined variation of the SFV method mesh is used in order to have the same number of degrees-of-freedom (DOF) as the SFV method solution. Further details of these tests, such as convergence conditions, can be seen in Breviglieri *et al.* (2014).

Pressure coefficient (C_p) distributions for these test cases, still considering $M_\infty = 0.8$ and $\alpha = 0$ deg., are shown in Fig. 5. Pressure coefficient distributions from experimental data (McDevitt and Okuno, 1985) are also shown in this figure. The experimental data contain a smooth transonic shock, due to shock wave-boundary layer interaction. This physical phenomenon cannot be reproduced in the numerical simulation since the Euler equations are being used.

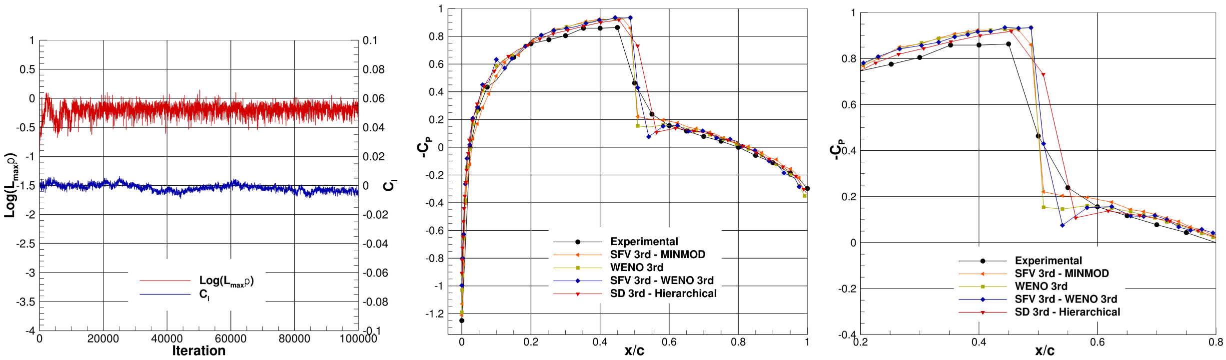

(a) Convergende history. (b) Complete airfoil C_p distribution. (c) Detail of the shock region C_p distribution.

Figure 5. Convergende data and C_p distributions comparison for the NACA 0012 airfoil at $M_\infty = 0.8$ and $\alpha = 0$ deg.

The best overall solution is provided by the WENO scheme. It accurately captures the shock and closely approximates the stagnation point. The only other method to provide a reasonably accurate stagnation pressure was the SFV scheme with the minmod limiter. A lack of good definition of the stagnation point appears on the solutions with the SFV-WENO and the SD methods. The common feature in both methods is the use of the AP-TDV marker, which is, then, thought to be responsible for this effect. In the shock region, the WENO scheme is able to capture a sharper discontinuity than the other methods. The SFV-minmod scheme generates a slightly weaker shock than expected, while the SFV-WENO solution significantly undershoots the pressure coefficient after the shock. The solution provided by the SD method does not capture the discontinuity as sharply as the WENO scheme and it presents a slight undershoot of the pressure coefficient downstream of the shock. Despite this difficulty in the definition of the shock region, the SD method provides one of the best solutions in the smooth regions. The SFV-WENO scheme can be slightly oscillatory and the SFV-minmod method is further away from the experimental data than the other methods in the region after the shock.

4.3 RAE 2822 Airfoil

Another reference aeronautical flow simulated is the transonic flow over a RAE 2822 supercritical airfoil. In this case, the airfoil profile is set with 2.31 deg. angle-of-attack in relation to the freestream, with a freestream Mach number of $M_\infty = 0.729$. The computational mesh used has a *C*-type grid topology and the farfield boundary is set at 100 chords from the airfoil. The mesh is composed of 7254 quadrilateral cells, of which 186 edges lie on the airfoil surface, as necessary to properly describe the airfoil geometry. These edges are concentrated in the airfoil leading edge and finite trailing edge, which contains 39 cell edges.

The flow is simulated with a 3rd-order SD scheme coupled with the hierarchical limiter formulation. Results obtained for this case are shown in Fig. 6 in the form of density contours and of a visualization of the limited cells for density reconstruction in the last iteration. The presence of a shock wave along the upper surface of the airfoil is clear, while the lower surface solution remains smooth, as also observed in Slater (2015). As in the NACA 0012 airfoil simulations, the limiter is active in regions of the flow in which the solution is apparently smooth. This observation suggests that the limiting procedure taking place in these cells is not affecting the physics of the solution, but only satisfying a numerical condition.

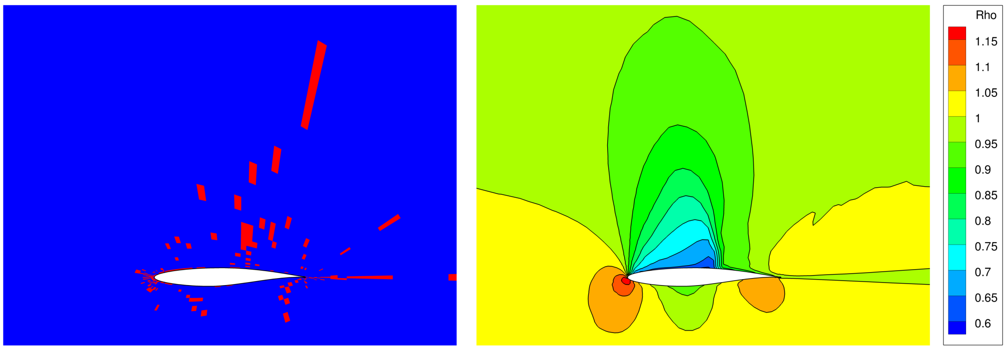

(a) Limited cells for density reconstruction (red). (b) Density contours.

Figure 6. Results for the SD method RAE 2822 airfoil simulations at $M_\infty = 0.729$ and $\alpha = 2.31$ deg.

In this simulation, a significant residue drop is observed, differently from the behavior seen in the NACA 0012 transonic flow calculations. Nevertheless, one can see that formal convergence, based on the L_∞ norm of the density residuals, stalls after almost 3 orders of magnitude drop in the residue, as indicated in Fig. 7(a). Lift coefficient convergence is again shown in the figure, further confirming solution convergence. The lift coefficient stabilizes at values between 0.80 and 0.81, after approximately $70,000$ iterations, similarly to results obtained in Breviglieri *et al.* (2014).

A comparison of the present results with those provided by the SFV method, coupled with three different limiting procedures, is performed. The tested limiters are a standard minmod limiter, a hybrid SFV-WENO scheme (Breviglieri *et al.*, 2014) and a hierarchical limiter (Breviglieri *et al.*, 2010). An unstructured grid is used for the SFV method simulations, and it is composed of 5378 triangles, of which 132 edges define the airfoil geometry. Differently from the SD method airfoil geometry, which has a closed trailing edge, the configuration used for the SFV method solutions has an open trailing edge. The grid is asymmetric and the distance from the airfoil to the farfield is of 100 chords. Further details of the simulations with the SFV method, such as convergence criteria, can be seen in Breviglieri *et al.* (2014).

Pressure coefficient (C_p) distributions are shown in Fig. 7. Experimental results are obtained from Slater (2015). Some differences from the experimental data are expected since the smooth transonic shock, caused by interaction with the boundary layer, cannot be represented in an Euler simulation. The resolution of the shock region by the 3rd-order SD method solution is significantly better than that provided with the 3rd-order SFV method, when coupled with high-order limiters. The SD method solution presents a shock closer to the experimental location and no undershooting is observed when compared to the SFV-WENO and SFV-hierarchical limiter schemes. The SFV-minmod method provides the best solution to the shock region, but at the cost of significant undershooting on the suction surface when compared to the SD method solution. The SFV-WENO and SFV-hierarchical limiter formulations show a large overshoot along the entire suction region. On the stagnation point, the SD method solution indicates a smaller stagnation pressure than the other methods tested or the experimental data. This behavior is attributed to incorrect limiting in this region. However, along other smooth regions of the flow, the solution produced by the SD method is never worse than the one provided by the SFV method with high-order limiters. The overall solution provided by the SD method is comparable to the results given

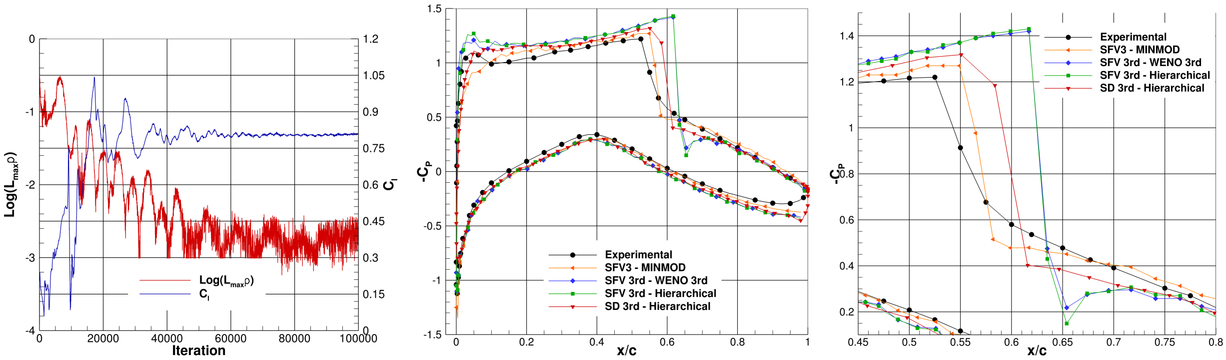

(a) Convergende history. (b) Complete airfoil C_p distribution. (c) Detail of the shock region C_p distribution.

Figure 7. Convergence data and C_p distributions comparison for the RAE 2822 airfoil at $M_\infty = 0.729$ and $\alpha = 2.31$ deg.

by SVF-minmod scheme. While the latter gives a more accurate result for the stagnation point, the former provides a better resolution for the expected pressure coefficient distribution along the suction region. The resolution of the shock is acceptable in both cases, especially considering the inviscid nature of these simulations.

4.4 Supersonic Flow Over a Wedge

In this test case, a uniform supersonic flow encounters a wedge with a 20 deg. half-angle, forming a steady oblique shock wave. The computational domain is 2 dimensionless units both in height and width. It is bounded by a supersonic inflow condition on its left edge, an inviscid wall boundary on the bottom and a supersonic outflow condition on both the right and top boundaries. The leading edge of the wedge is positioned at half of the horizontal length of the domain in order to ensure the shock wave leaves the computational domain through the right boundary. In the present simulations, a freestream Mach number $M_\infty = 2.0$ incident flow is considered.

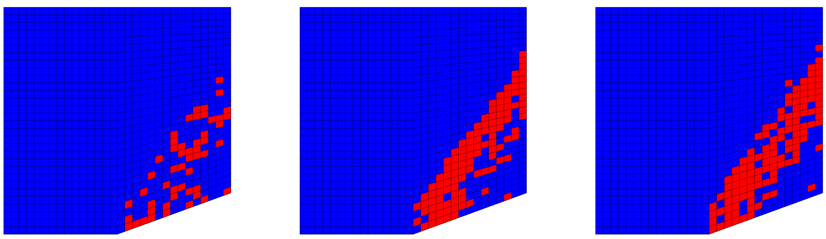

(a) 2nd-order method marker. (b) 3rd-order method marker. (c) 4th-order method marker.

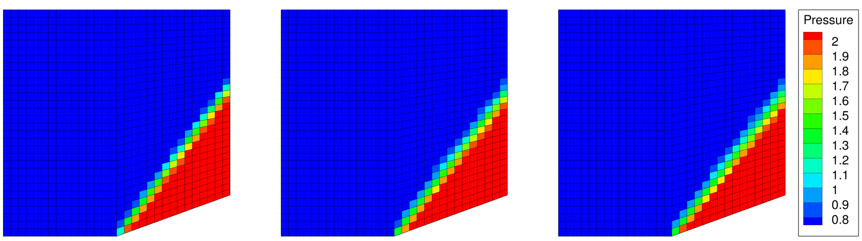

(d) 2nd-order method. (e) 3rd-order method. (f) 4th-order method.

Figure 8. Limiter marked cells, in red, on the last iteration and pressure contours for the flow over a wedge.

The solutions obtained are presented in form of cell averaged pressure contours for 2nd-, 3rd- and 4th-order schemes and they are shown in Fig. 8. The results are obtained with the maximum CFL values allowed by the Runge-Kutta scheme and, thus, demonstrate the robustness of the limiter. Shock angle is also in good agreement with theoretical value. However, due to the coarse nature of the meshes, a precise measurement is rather difficult to be made.

The behavior of the marker is illustrated in Fig. 8, where the limited cells in the last iteration are marked in red. It can be observed that, despite effective, the marker does not limit the entire shock on all iterations. This is more pronounced in the 2nd-order case, in which an oscillatory behavior is observed. This effect is believed to be caused by overzealous limiting that prevents the shock from reappearing for a few iterations. The increase in the number of marked cells in higher order cases is possibly caused by the higher-order polynomial interpolation procedures.

5. CONCLUDING REMARKS

The paper presents results for an implementation of the high-order SD method for inviscid flows. The SD method uses a simple universal reconstruction to produce high-order polynomial approximations of the solution. Accuracy evaluations, such as those using the Ringleb flow problem, demonstrate the capability of the method to provide solutions with the expected accuracy. A high-order limiter formulation is used with the intent of preserving the maximum possible order of accuracy in discontinuous solutions and simulation of reference aeronautic transonic flows verify the applicability and accuracy of the SD method and the hierarchical limiter for the flows of interest. Results show some disadvantages over the SFV method, with a low-order limiter, and WENO schemes, especially at stagnation points and shock regions. Nonetheless, improvements over previous applications of high-order limiters, used together with the SFV method, are clear. The same simulations also reveal unexpected behaviour of the oscillation marker, such as an over-sensitivity in smooth regions of the flow and excessive marking near wall boundaries. This can possibly cause unwanted triggering of the limiter that affects not only the solution but also the convergence properties of the simulation.

Comparison of the results in this paper with a SD method coupled to a low order limiter may provide further guidance. Moreover, other efforts should be directed to convergence rate improvements and high-order geometric representation. These are fundamental for the efficient use of any high-order method.

ACKNOWLEDGEMENTS

The authors gratefully acknowledge the partial support for this research provided by Conselho Nacional de Desenvolvimento Científico e Tecnológico, CNPq, under the Research Grants No. 309985/2013-7, No. 400844/2014-1, No. 443839/2014-0 and No. 574004/2008-4. This work is also supported by Fundação Coordenação de Aperfeiçoamento de Pessoal de Nível Superior, CAPES, through a M.Sc. scholarship for the first author. The authors are also indebted to the partial financial support received from Fundação de Amparo à Pesquisa do Estado de São Paulo, FAPESP, under the Research Grants No. 2008/57866-1 and No. 2013/07375-0.

6. REFERENCES

Breviglieri, C., Azevedo, J.L.F., Basso, E. and Souza, M.A.F., 2010. "Implicit high-order spectral finite volume method for inviscid compressible flows". *AIAA Journal*, Vol. 48, No. 10, pp. 2365–2376.

Breviglieri, C., Paula, L.G.L., Moreira, F.M., Wolf, W.R. and Azevedo, J.L.F., 2014. "A comparative study of discontinuous high order methods for compressible flows". In AIAA Paper No. 2014-2984*, 32nd AIAA Applied Aerodynamics Conference*. Atlanta, GA.

May, G. and Jameson, A., 2006. "A spectral difference method for the Euler and Navier-Stokes equations on unstructured meshes". In *44th AIAA Aerospace Sciences Meeting*. AIAA Paper No. 2006-304, Reno, NV.

McDevitt, J. and Okuno, A.F., 1985. "Static and dynamic pressure measurements on a NACA 0012 airfoil in the Ames High Reynolds Number Facility". NASA TP-2485, NASA.

Moreira, F.M., Breviglieri, C. and Azevedo, J.L.F., 2015. "High-order compressible flows simulations with the unstructured spectral difference method". In *Proceedings of the 22nd AIAA Computational Fluid Dynamics Conference*. Dallas, TX.

Shapiro, A.H., 1953. *The Dynamics and Thermodynamics of Compressible Fluid Flow*. Wiley, New York.

Slater, J.W., 2015. "NPARC Alliance Validation Archive". http://www.grc.nasa.gov/WWW/wind/valid/raetaf/raetaf.html.

Spitieri, R.J. and Ruuth, S.J., 2003. "A new class of optimal high-order strong-stability-preserving time discretization methods". *SIAM Journal on Numerical Analysis*, Vol. 40, No. 2, pp. 469–491.

van den Abeele, K., Lacor, C. and Wang, Z.J., 2008. "On the stability and accuracy of the spectral difference method". *J. Sci. Comput.*, Vol. 37, pp. 162–188.

Wang, Z.J., Fidkowski, K., Abgrall, R., Bassi, F., Caraeni, D., Cary, A., Deconinck, H., Hartmann, R., Hillewaert, K., Huynh, H.T., Kroll, N., May, G., Persson, P., van Leer, B. and Visbal, M., 2013. "High-order CFD methods: Current status and perspective". *Int. J. Numer. Meth. Fluids*, Vol. 72, No. 8, pp. 811–845.

Wang, Z.J., Liu, Y., May, G. and Jameson, A., 2007. "Spectral difference method for unstructured grids II: Extension to the Euler equations". *Journal of Scientific Computing*, Vol. 32, No. 1.

Wolf, W.R. and Azevedo, J.L.F., 2007. "High-order ENO and WENO schemes for unstructured grids". *Int. J. Numer. Meth. Fluids*, Vol. 55, No. 10, pp. 917–943.

Yang, M. and Wang, Z.J., 2009. "A parameter-free generalized moment limiter for high-order methods on unstructured grids". *Advances in Applied Mathematics and Mechanics*, Vol. 1, No. 4, pp. 451–480.

7. RESPONSIBILITY NOTICE

The authors are the only responsible for the printed material included in this paper.